Supplementary Information

Modifying the electronic properties of single-walled carbon nanotubes using designed surfactant peptides

Dinushi R. Samarajeewa, Gregg R. Dieckmann, Steven O. Nielsen and Inga H. Musselman*

Department of Chemistry, The University of Texas at Dallas, 800 West Campbell Road, Richardson, Texas 75080, USA.
Fax: +1 972 883 2925; Tel: +1 972 883 2706; E-mail: imusselm@utdallas.edu

Table S1. Characteristics of the surfactant peptides. [a]Expected molecular weights calculated based on the amino acid composition and [b]experimental values obtained from MALDI-TOF MS analysis (analysis done by The University of Alabama, Tuscaloosa, AL). [c]Retention times of the surfactant peptides measured using a Hewlett-Packard HP1100 DAD reversed-phase high performance liquid chromatography (RP-HPLC) system, equipped with a Themo-Finnigan C4 reversed-phase column. Gradient elution was performed with 'solvent A', containing 99.9% water and 0.1% TFA, and 'solvent B', containing 90% ACN, 9.9% water, and 0.1% TFA.

Surfactant peptide	Expected molecular weight[a] ($g\ mol^{-1}$)	m/z values obtained from MALDI-TOF MS[b]	Retention times by RP-HPLC[c] (min)
SPF	958.2	958.9	34.8
SP-*p*NH_2F	973.2	973.8	23.4
SP-*p*CNF	983.3	983.9	33.5

Determination of the molar extinction coefficients of aromatic test amino acids. Standard calibration curves were constructed using Beer's law to determine the molar extinction coefficients of the test amino acids. For H-Phe-OH, a concentration series ranging from 1.0×10^{-3} to 4.0×10^{-3} M was prepared, and the absorbances were measured at 257 nm (Figure S1a) using a Cary 50 Bio UV-Vis-NIR spectrometer. For H-Phe[4-NH_2]-OH and H-Phe[4-CN]-OH, a concentration series ranging from 2.0×10^{-4} to 10.0×10^{-4} M was prepared, and the corresponding absorbances were recorded at 285 nm and at 271 nm, respectively (Figures S1b-c, respectively). Data acquisition was carried out using nanopure water as the blank. For each amino acid, 4 separate trials were performed to ensure reproducibility. Molar extinction coefficients were calculated from the slopes of the calibration plots: $\varepsilon_{\text{phenylalanine}} = 193 \pm 8$ L mol^{-1} cm^{-1} (at 257 nm), $\varepsilon_{p\text{-amino-phenylalanine}} = 1333 \pm 8$ L mol^{-1} cm^{-1} (at 285 nm), and $\varepsilon_{p\text{-cyano-phenylalanine}} = 761 \pm 3$ L mol^{-1} cm^{-1} (at 271 nm).

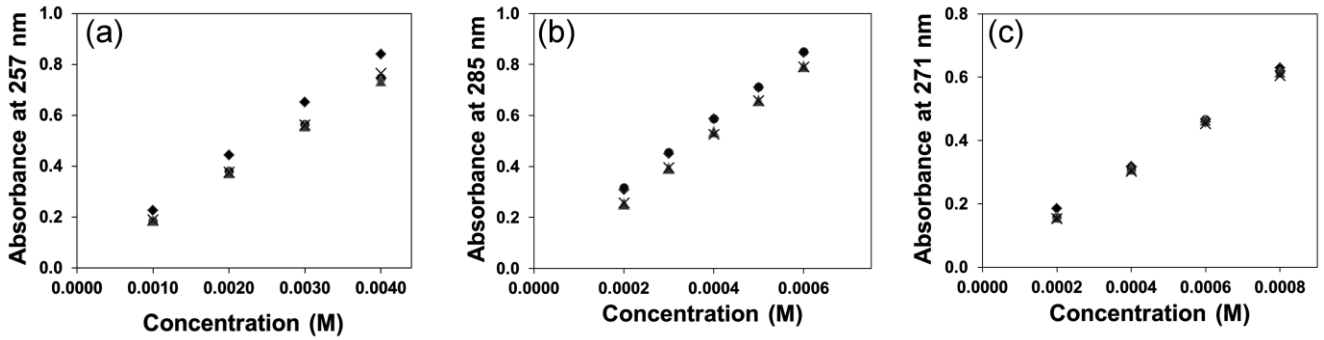

Figure S1. Beer's law standard calibration curves for aromatic amino acids: (a) phenylalanine, (b) *p*-amino-phenylalanine, and (c) *p*-cyano-phenylalanine. Each graph presents 4 separate trials.

Determination of optimum surfactant peptide concentration for the preparation of SWCNT dispersions. SPF/SWCNT dispersions were prepared with varying the concentrations of the peptide solutions (100-500 μM). The AFM image of the 20-fold diluted 500 μM SPF/SWCNT (Figure S2 d) sample shows a significant number of SWCNTs as compared to dispersions prepared with lower peptide concentrations.

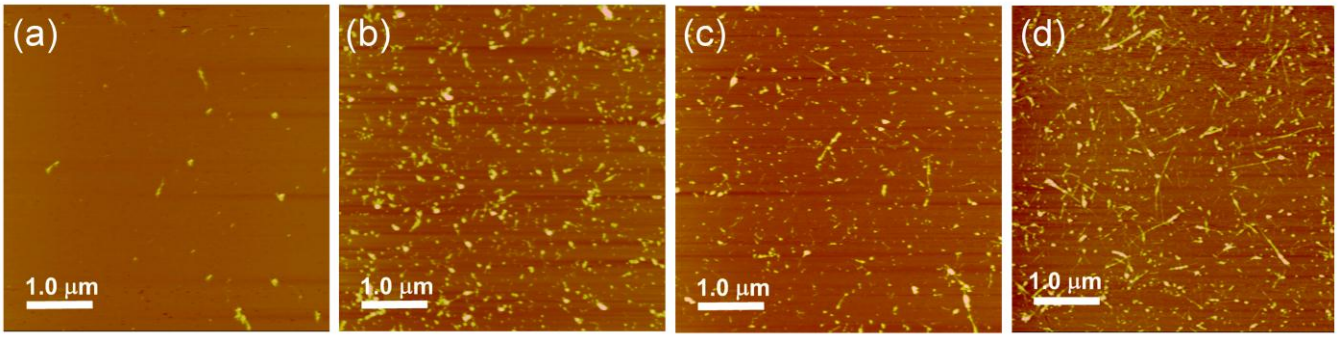

Figure S2. AFM images (5.0 x 5.0 μm) of SPF/SWCNT dispersions centrifuged at 50,000 x g; (a) 100 μM SPF/SWCNT, (b) 200 μM SPF/SWCNT, (c) 300 μM SPF/SWCNT, and (d) 500 μM SPF/SWCNT. The dispersions were diluted 20-fold with nanopure water and dried 24 h before imaging.

Determination of optimum centrifugation speed for the preparation of SWCNT dispersions. AFM images were acquired from 500 μM surfactant peptide/SWCNT dispersions collected after centrifugation at 4 speeds; 16,000 × g, 20,000 × g, 50,000 × g, and 100,000 × g. Dispersions collected after the 100,000 × g spin exhibit clean backgrounds with less particulate matter and less excess peptide as compared to the other samples.

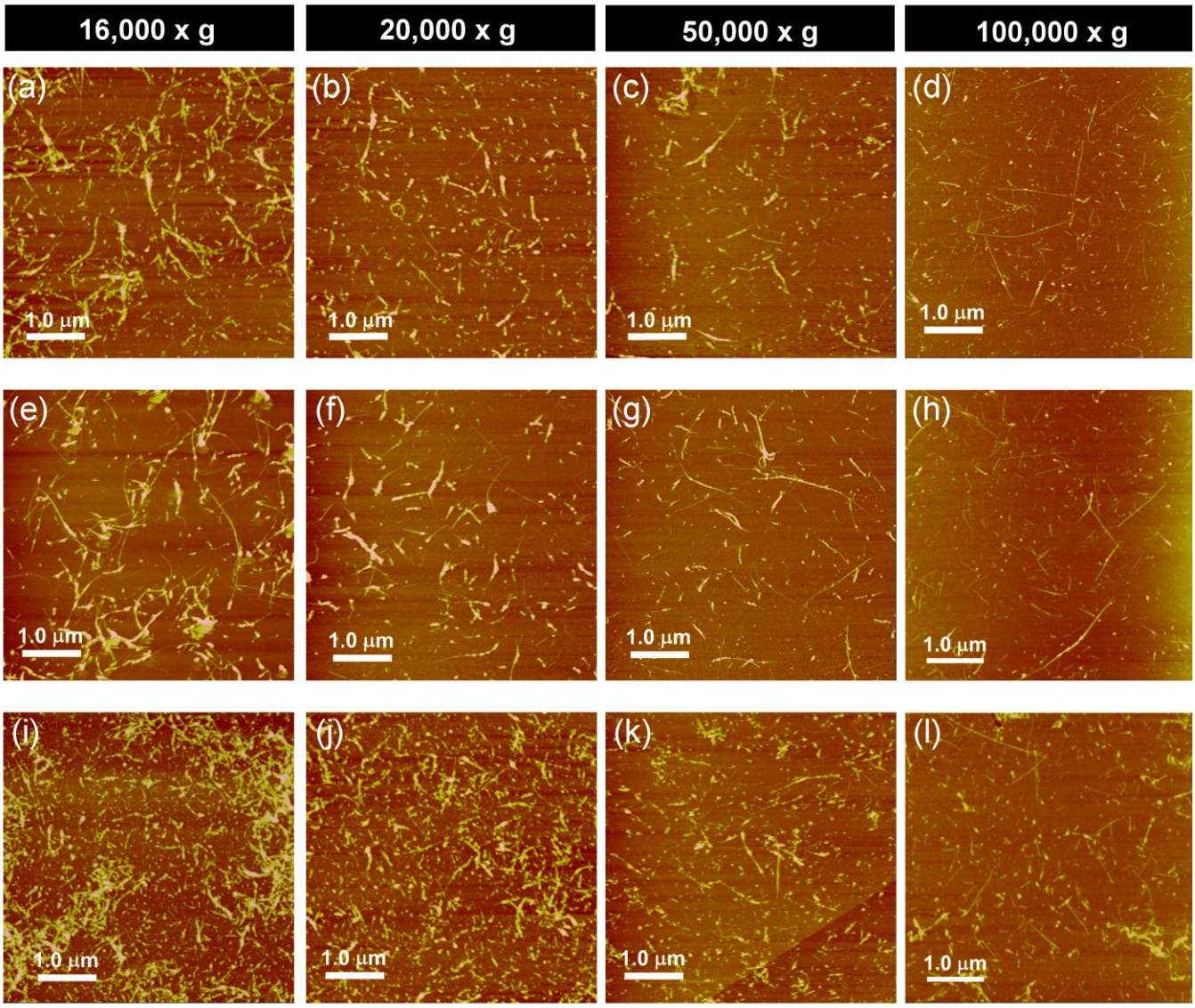

Figure S3. AFM images (5.0 x 5.0 μm) of 20-fold diluted 500 μM surfactant peptide/SWCNT dispersions after centrifugation at different speeds. Top row: SPF/SWCNT (a-d), middle row: SP-*p*NH_2F/SWCNT (e-h), and bottom row: SP-*p*CNF/SWCNT (i-l).

Absorption spectra of surfactant peptide/SWCNT dispersions as a function of centrifugation speed. UV-Vis-NIR spectroscopy was performed on 500 μM surfactant peptide/SWCNT dispersions collected after centrifugation at different speeds. Spectra acquired from the dispersions spun at 100,000 × g show prominent peaks as compared to the other samples. The absorption spectra obtained from the SP-*p*NH_2F/SWCNT composite exhibit more intense peaks with respect to the other composites.

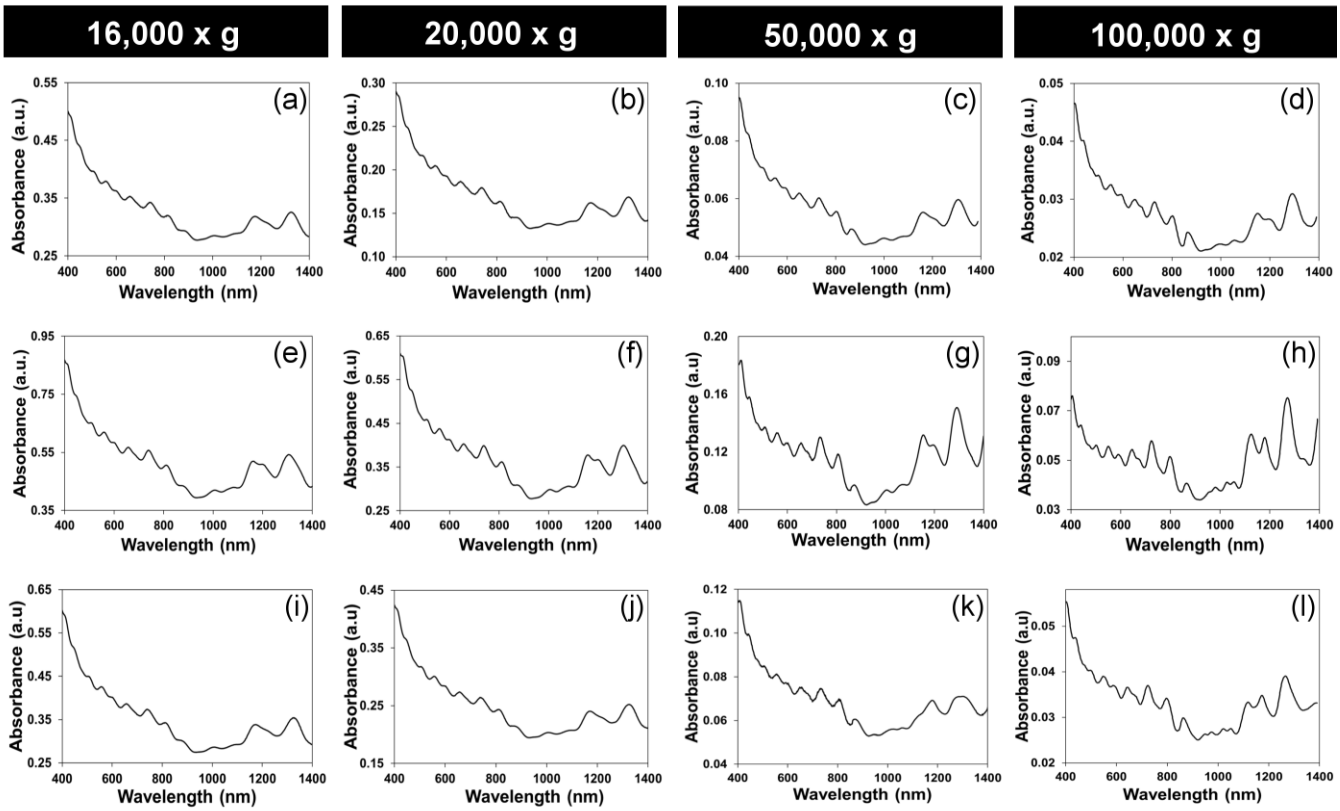

Figure S4. UV-Vis-NIR spectra of 500 μM surfactant peptide/SWCNT dispersions collected after centrifugation at different speeds. Top row: SPF/SWCNT (a-d), middle row: SP-*p*NH_2F/SWCNT (e-h), and bottom row: SP-*p*CNF/SWCNT (i-l).

Chirality assignments of surfactant peptide/SWCNT composites and corresponding absorption peak shifts. Table S2 presents the wavelengths of the absorption peaks and the assigned (n,m) chiral indices. The chirality assignments were made using the wavelengths corresponding to the first van Hove optical transitions determined from UV-Vis-NIR absorbance data. Peak fitting was performed using PeakFit v4.12. The (n,m) chiralities were assigned based on the reported data for SDS-dispersed SWCNTs.[1] For several wavelengths, there were more than one possible chirality assignment.

Table S2. UV-Vis-NIR absorption peak positions of surfactant peptide/SWCNT composites and the corresponding SWCNT chirality assignments.

	SPF/SWCNT	SP-*p*NH_2F/SWCNT	SP-*p*CNF/SWCNT	Assigned chiral indices (n,m)	SDS/SWCNT[a]
Absorption peaks (nm)		1316		(13,2)	1308
	1298	1273	1273	(8,7)	1268
	1204	1183	1180	(8,6) (12,1)	1173, 1172
	1155	1127	1124	(7,6) (8,4)	1123, 1114
	1057	1060	1056	(10,2)	1055
		1031	1026	(7,5)	1024
	994	984	980	(6,5) (7,3)	976
	943	957	951	(8,3)	953
	874	870	872	(6,4)	874
	808	805	805	(12,1)	798
		761	763		
	733	728	728	(10,2) (8,7)	735,729
	680	681	679	(8,3) (9,5)	664,672
		648	649	(7,5) (7,6)	645,648
	596	599	596	(8,4)	588
	557	557	557	(6,5) (9,2)	568,552
	509	507	507	(7,3)	504
			473		
	445	446	445		
	408	409	408		

[a]corresponding wavelength values for the assigned (n,m) chiralities.[1]

The absorption spectra, in general, have distinct regions corresponding to the electronic transitions of semiconducting (E_{11}^S: 800-1600, E_{22}^S: 500-900) and metallic (E_{11}^M: 400-600) nanotubes.[2] Factors such as the existence of SWCNT bundles, as well as different dielectric environments nearby the SWCNTs,

may cause a shift in these absorption peaks.[3,4] The values present in Table S2 clearly show that the peaks in the region of ~400 to 900 nm are almost completely overlapping for the different surfactant peptide/SWCNT composites, in contrast to some peaks in the region of ~900 to 1300 nm, wherein significant peak shifting is evident. Literature reports suggest that the absorption peaks corresponding to the electronic transitions of semiconducting tubes are more prone to shifts than those of metallic tubes because the electronic transitions of the latter type are shielded from their surroundings owing to the Fermi electron screening effect.[1,5] Shifts observed in the region of ~720 to 900 nm are diminutive, and it is not possible to identify whether these result from different dielectric environments in the vicinity of the SWCNTs or from errors associated with the peak fitting method (1 to 3 nm shifts in data).

As can be seen from the data, most absorption peaks for SPF/SWCNTs in the E_{11}^{S} region exhibit red-shifting with respect to the other two spectra. For example, red-shifts observed for SPF/SWCNT peaks at 1298 nm, 1204 nm, and 1155 nm are in the range of 21-30 nm and for the peak at 994 nm it is around 10-15 nm with respect to the corresponding absorbance peaks of SP-*p*NH_2F/SWCNT and SP-*p*CNF/SWCNT. However, the SPF/SWCNT peak at 943 nm is blue-shifted with respect to the other two peptides. At this wavelength, SP-*p*NH_2F/SWCNT is red-shifted by about 14 nm, whereas for SP-*p*CNF/SWCNT the red-shift is ~8 nm with respect to SPF/SWCNT. Shifts observed for the rest of the peaks are less than 4 nm and, hence, are not used for the comparison since such small variations can be induced from experimental errors. Typically, absorption peak shifts to higher wavelengths (red-shift) indicate the presence of bundled SWCNTs in samples.[3,6] Even though the red-shifting of the SPF/SWCNT absorption peaks, as well as the suppression of the peak intensities as compared to the other two composites, might suggest that the SWCNTs in SPF/SWCNT dispersions are bundled, this is likely not the case since AFM height analysis confirmed that all three surfactant peptide/SWCNT dispersions mostly contained singly dispersed SWCNTs. Several studies have reported that the adsorption of aromatic molecules onto SWCNT surfaces leads to the red-shifting of their absorption

peaks, owing to the reduction of the excitonic optical transition energies of the nanotube.[3,7] However, compared to SPF/SWCNT, the blue-shifts observed for the SP-*p*NH_2F/SWCNT and SP-*p*CNF/SWCNT composites presumably result from the different dielectric environments created by the peptides themselves due to the presence of electron-donating or electron-withdrawing groups on their aromatic ring.

The interaction of SWCNTs with electron-donors or electron-acceptors is known to modulate absorption peaks due to alterations that occur in the electronic transitions.[8-10] Specifically, the disappearance of absorption peaks, as well as the appearance of new peaks, were reported for doped SWCNTs.[8-10] These studies reveal that both electron-donors and electron-acceptors have similar optical effects.[10] In the current study, even though peak suppression is not observed, a new peak is identified in both SP-*p*NH_2F/SWCNT and SP-*p*CNF/SWCNT spectra in the region of ~1026-1031 nm. This peak could be a doping-induced absorption feature, since it was not present in the SPF/SWCNT spectrum. However, further studies need to be performed in order to confirm this behavior. The other difference observed with the SP-*p*NH_2F/SWCNT and SP-*p*CNF/SWCNT spectra, compared to the SPF/SWCNT spectrum, is the shifting of the absorption peaks to lower wavelengths. Even though both SP-*p*NH_2F and SP-*p*CNF-coated SWCNTs show a blue-shift relative to the reference, the SP-*p*NH_2F/SWCNT peaks are slightly red-shifted (by ~3-6 nm) compared to SP-*p*CNF/SWCNT. Such a shifting pattern has not been previously reported for dopant/SWCNT composites. However, Kim et al. observed a shift in an E_{22}^S peak to higher energy for SWCNTs doped with $AuCl_3$, wherein Au^{3+} adsorbed SWCNT composites behaved as *p*-doped materials.[9] On the other hand, Voggu and coworkers showed that a peak observed in the E_{22}^S region shifted in the opposite direction for aniline/SWCNT and nitro-benzene/SWCNT composites as compared to the reference benzene/SWCNT composite.[11] Similar shifting pattern was observed by Ghosh *et al.* for SWCNT composites functionalized with aromatic donor and acceptor

molecules.[12] Nevertheless, at present, it is not well understood why both SP-*p*NH_2F/SWCNT and SP-*p*CNF/SWCNT composites show a blue shift as compared to the reference SPF/SWCNT.

Reproducibility of Raman G-band peak positions of surfactant peptide/SWCNT composites. Raman spectra were acquired from three separately prepared dispersions of each composite. G-band peak positions obtained from each trial of each composite (Table S3) show only slight variation confirming the reproducibility of data acquisition.

Table S3. Raman G-band peak positions and average G-band peak shifts of the surfactant peptide-coated SWCNTs. Average peak shifts were calculated with respect to the G-band peak position of the SPF/SWCNT composite. Data were acquired from three separately prepared dispersions. Two additional trials were performed on one set of dispersions.

Dispersion, Trial	SP-*p*NH_2F/ SWCNT (cm^{-1})	SPF/SWCNT (cm^{-1})	SP-*p*CNF/ SWCNT (cm^{-1})
Dispersion 1, Trial 1	1589.93	1591.94	1592.92
Trial 2	1589.92	1591.51	1592.84
Trial 3	1589.53	1591.79	1592.90
Dispersion 2, Trial 1	1590.27	1591.77	1592.79
Dispersion 3, Trial 1	1589.87	1591.78	1592.85
Average G-band peak value	1589.90 ± 0.26	1591.70 ± 0.12	1592.86 ± 0.05
Average shift with respect to SPF/SWCNT	-1.80 ± 0.30	-	1.16 ± 0.14

STM/STS data acquisition from standard substrates. Highly oriented pyrolytic graphite (HOPG) and Au(111)-coated mica substrates were primarily used to verify the accuracy of STM/STS data acquisition (Figure S5). I-V curves acquired from HOPG show a rectifying behavior, whereas the I-V curves of Au(111)-coated mica substrates exhibit an ohmic behavior. The averaged I-V data (n=20) were numerically converted to the equivalent differential conductance (dI/dV) spectra, which are proportional to the LDOS of materials.

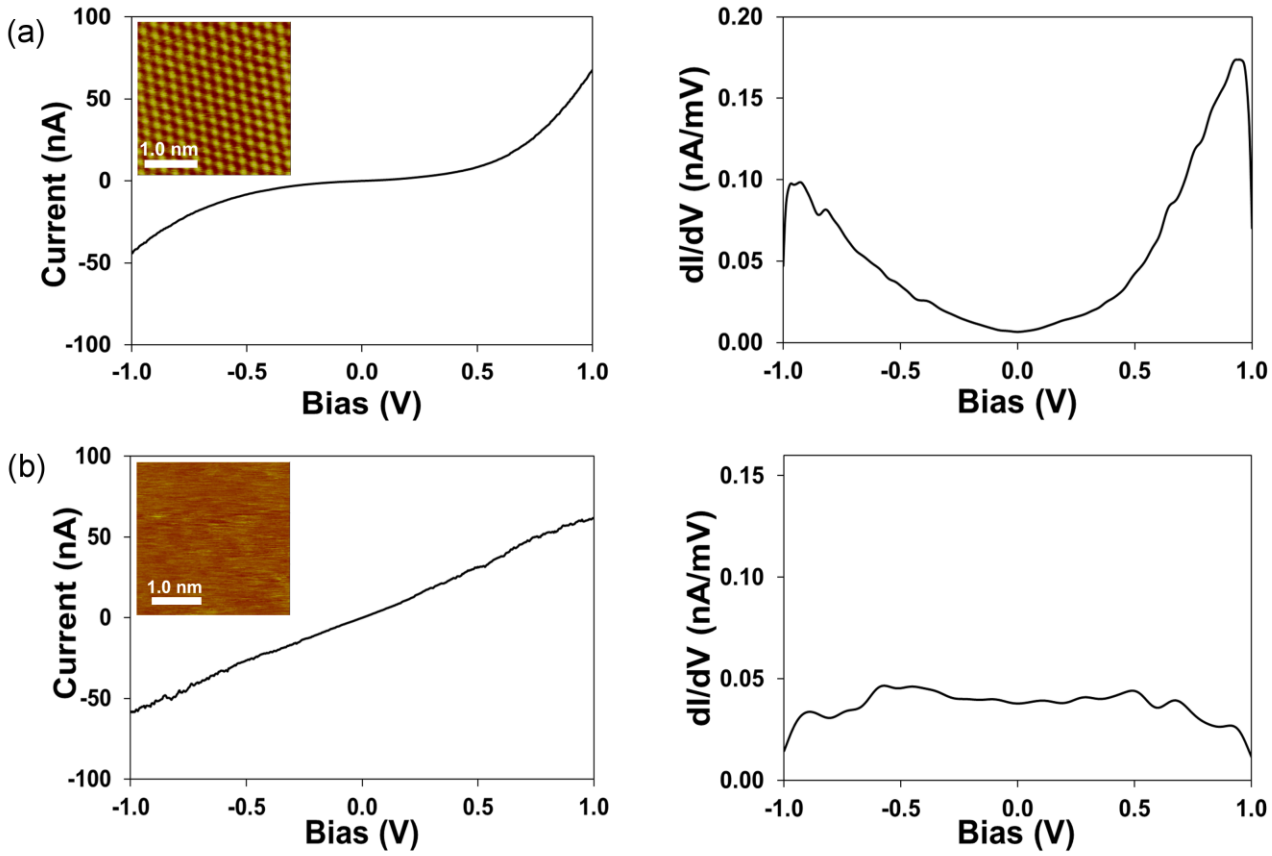

Figure S5. STS I-V curves and corresponding STS dI/dV spectra of the substrates. (a) I-V curve (left) and STS dI/dV spectrum (right) of HOPG. Inset: STM image of HOPG surface. (b) I-V curve (left) and STS dI/dV spectrum (right) of Au(111)-coated mica. Inset: STM image of Au surface.

STM/STS data acquisition from surfactant peptide controls. Figure S6 presents STM images and the equivalent STS dI/dV spectra of the surfactant peptide control samples on Au(111) substrates. As can be observed, the STS dI/dV spectra of the peptide controls (Figure S6 right column) are virtually featureless, demonstrating that peptide contributions to the density of states in this bias range (-1.0 to 1.0 V) are minimal.

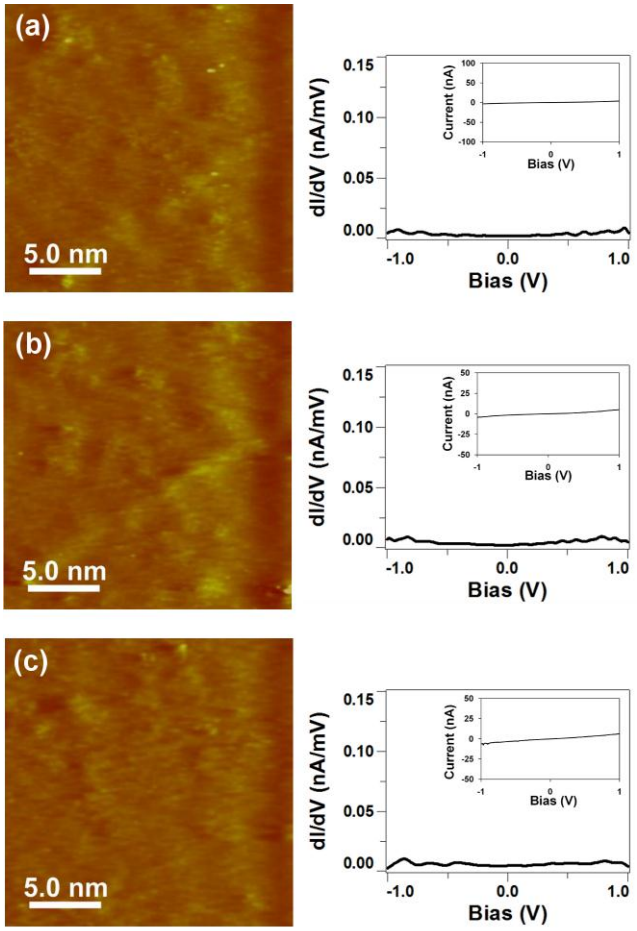

Figure S6. STM images (left column) and corresponding STS dI/dV spectra (right column) of surfactant peptide control samples spun-cast onto Au(111) substrates. (a) SPF, (b) SP-*p*NH_2F, and (c) SP-*p*CNF. The STM images exhibited no SWCNT-like features. The insets in the dI/dV spectra are the equivalent I-V curves.

Preparation of 1,2-dichloroethane/SWCNT (DCE/SWCNT) dispersions. To prepare dispersions, 3.0 mg of HiPco SWCNTs were mixed with 6 mL of 1,2-DCE and vortexed for 5 min. Then, the sample was bath sonicated (Cole-Parmer 8890) for ~5 h and allowed to settle for 2 d. Subsequently, 1 mL of the mixture was pipetted into an Eppendorf tube and probe sonicated for 2 min using a VWR Scientific Branson Sonifier at a power level of 10 W, with the sample immersed in an ice water bath. The dispersion was then centrifuged at 16,000 x g for 30 min in an Eppendorf 5417C centrifuge and the upper 50% of the supernatant was recovered. For the AFM analysis of bare nanotubes, 20 μL of the supernatant was spun-cast (3500 rpm, 30 s) onto a freshly cleaved mica substrate and dried in a desiccator. Figure S7 shows a resultant AFM image, wherein both individual SWCNTs and SWCNT bundles are evident.

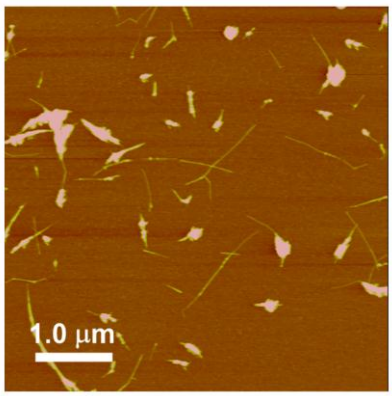

Figure S7. An AFM image (5.0 x 5.0 μm) of SWCNTs dispersed with 1,2-dichloroethane.

Table S4. Peak positions of additional features near the Fermi-level (-0.20 to 0.20 V) observed in STS dI/dV spectra of semiconducting SWCNTs. (a) Uncoated SWCNTs, (b) SPF/SWCNTs, (c) SP-*p*NH_2F/SWCNTs, and (d) SP-*p*CNF/SWCNTs. (VB and CB stand for valence band side and conduction band side, respectively.)

(a) Uncoated SWCNTs (semiconducting)		
SWCNT #	VB	CB
1	-	-
2	-	-
3	-	-
4	-	-
5	-	-
6	-	-
7	-	-
8	-	-
9	-	-
10	-	-
11	-	-
12	-	-
13	-0.18	0.19

(b) SPF/SWCNT (semiconducting)		
SWCNT #	VB	CB
1	-	-
2	-	-
3	-	-
4	-	-
5	-	-
6	-	-
7	-	-
8	-	-
9	-	-
10	-	-
11	-	-
12	-0.15	0.14

(c) SP-pNH_2F/SWCNT (semiconducting)

SWCNT #	VB	CB	SWCNT #	VB	CB
1	-	0.18	15	-	-
2	-	0.18	16	-	-
3	-	0.12	17	-	-
4	-	0.10	18	-	-
5	-	0.14	19	-	-
6	-	0.17	20	-	-
7	-	0.17	21	-	-
8	-	0.20	22	-	-
9	-	0.15	23	-	-
10	-	0.16	24	-	-
11	-	0.15	25	-	-
12	-	0.09	26	-	-
13	-	-	27	-0.20	0.18
14	-	-	28	-0.09	0.15

(d) SP-pCNF/SWCNT (semiconducting)

SWCNT #	VB	CB	SWCNT #	VB	CB
1	-0.19	-	16	-	-
2	-0.12	-	17	-	-
3	-0.12	-	18	-	-
4	-0.14	-	19	-	-
5	-0.09	-	20	-	-
6	-0.09, -0.17	-	21	-	-
7	-0.10	-	22	-	-
8	-0.09	-	23	-	-
9	-0.11	-	24	-	-
10	-	-	25	-	-
11	-	-	26	-	-
12	-	-	27	-0.13	0.15
13	-	-	28	-0.18	0.13
14	-	-	29	-0.17	0.12
15	-	-	30	-0.19	0.15

References

1 R. B. Weisman and S. M. Bachilo *Nano Lett*., 2003, **3**, 1235.

2 M. J. O'Connell, S. M. Bachilo, C. B. Huffman, V. C. Moore, M. S. Strano, E. H. Haroz, K. L. Rialon, P. J. Boul, W. H. Noon, C. Kittrell, J. Ma, R. H. Hauge, R. B. Weisman and R. E. Smalley, *Science*, 2002, **297**, 593.

3 H. Huang, H. Kajiura, R. Maruyama, K. Kadono and K. J. Noda, *Phys. Chem. B*, 2006, **110**, 4686.

4 F. Bonaccorso, *Intl. J. Photoenergy*, 2010, **2010**, Article ID 727134.

5 N. Nair, M. L. Usrey, W.-J. Kim, R. D. Braatz and M. S. Strano, *Anal. Chem*., 2006, **78**, 7689.

6 S. M. Tabakman, K. Welsher, G. Hong and H. Dai, *J. Phys. Chem. C*, 2010, **114**, 19569.

7 W. Fan and R. Zhang, *Sci. China. Ser. B-Chem*., 2008, **51**, 1203.

8 N. Minami, S. Kazaoui, R. Jacquemin, H. Yamawaki, K. Aoki, H. Kataura and Y. Achiba, *Synthetic Met*., 2001, **116**, 405.

9 K. K. Kim, J. J. Bae, H. K. Park, S. M. Kim, H.-Z. Geng, K. A. Park, H.-J. Shin, S.-M. Yoon, A. Benayad, J.-Y. Choi and Y. H. Lee, *J. Am. Chem. Soc*., 2008, **130**, 12757.

10 S. Kazaoui, N. Minami and R. Jacquemin, *Phys. Rev. B*, 1999, **60**, 13339.

11 R. Voggu, C. S. Rout, A. D. Franklin, T. S. Fisher and C. N. R. Rao, *J. Phys. Chem. C*, 2008, **112**, 13053.

12 A. Ghosh, K. V. Rao, R. Voggu and S. J. George, *Chem. Phys. Lett*., 2010, **488**, 198.